remote sensing

MDPI

Article

Vegetation Dynamic in a Large Floodplain Wetland: The Effects of Hydroclimatic Regime

Lei Jing [1,2,3], Qing Zeng [1], Ke He [1], Peizhong Liu [1], Rong Fan [1], Weizhi Lu [2], Guangchun Lei [1], Cai Lu [1,*] and Li Wen [4]

[1] School of Ecology and Nature Conservation, Beijing Forestry University, Beijing 100083, China; leijing@csuft.edu.cn (L.J.); zengqing@bjfu.edu.cn (Q.Z.); heke0611@bjfu.edu.cn (K.H.); peizhongliu@bjfu.edu.cn (P.L.); fanrong1119@bjfu.edu.cn (R.F.); leiguangchun@bjfu.edu.cn (G.L.)
[2] National Engineering Laboratory for Applied Technology of Forestry & Ecology in South China, Central South University of Forestry and Technology, Changsha 410004, China; weizhilu@csuft.edu.cn
[3] Key Laboratory of Soil and Water Conservation and Desertification Combating of Hunan Province, Central South University of Forestry and Technology, Changsha 410004, China
[4] Science, Economics, and Insights Division, Department of Planning and Environment, Lidcombe, NSW 2000, Australia; li.wen@environment.nsw.gov.au
* Correspondence: cailu@bjfu.edu.cn; Tel.: +86-010-6233639

Abstract: Floodplain wetlands are among the most dynamic ecosystems on Earth, featuring high biodiversity and productivity. They are also sensitive to anthropogenic disturbances and are globally threatened. Understanding how flow regime drives the spatiotemporal dynamics of wetland habitats is fundamental to effective conservation practices. In this study, using Landsat imagery and the random forest (RF) machine learning algorithm, we mapped the winter distribution of four wetland habitats (i.e., *Carex* meadow, reedbed, mudflat, and shallow water) in East Dongting Lake, a Ramsar wetland in the middle to lower Yangtze Basin of China, for 34 years (1988–2021). The dynamics of wetland habitats were explored through pixel-by-pixel comparisons. Further, the response of wetland habitats to flow regime variations was investigated using generalized additive mixed models (GAMM). Our results demonstrated the constant expansion of reedbeds and shrinkage of mudflats, and that there were three processes contributing to the reduction in mudflat: (1) permanent replacement by reedbed; (2) irreversible loss to water; and (3) transitional swapping with *Carex* meadow. These changes in the relative extent of wetland habitats may degrade the conservation function of the Ramsar wetland. Moreover, the duration of the dry season and the date of water level withdrawal were identified as the key flow regime parameters shaping the size of wetland habitats. However, different wetland vegetation showed distinct responses to variations in flow regime: while *Carex* meadow increased with earlier water withdrawal and a longer dry season, reedbed continuously expanded independent of the flow regime corresponding to the increase in winter rainfall. Our findings suggested that flow regime acts in concert with other factors, such as climate change and sand mining in river channels, driving wetland habitat transition in a floodplain landscape. Therefore, effective conservation can only be achieved through diverse restoration strategies addressing all drivers.

Keywords: wetland transition; random forest; singular spectrum analysis; generalized additive mixed models; time series; Phragmites encroachment

Citation: Jing, L.; Zeng, Q.; He, K.; Liu, P.; Fan, R.; Lu, W.; Lei, G.; Lu, C.; Wen, L. Vegetation Dynamic in a Large Floodplain Wetland: The Effects of Hydroclimatic Regime. *Remote Sens.* **2023**, *15*, 2614. https://doi.org/10.3390/rs15102614

Academic Editors: Chung-Te Chang and Junhu Dai

Received: 22 April 2023
Revised: 13 May 2023
Accepted: 14 May 2023
Published: 17 May 2023

1. Introduction

Floodplain wetlands of large rivers are among the most productive ecosystems, with rich biodiversity, and are of high ecological and socioeconomic importance [1–3]. Floodplains are also highly dynamic fluvial systems of great ecological complexity driven by periodic inundations associated with the high and low flows of the parent rivers (flood pulses) [4]. In a floodplain with natural hydrological regimes, wetlands are characterized

by their transience, being either vegetated (marshes and forest swamps), bare (mudflats), lentic (shallow lakes and lagoons) or lotic (channels) waters. The diverse hydrogeomorphic features of wetlands provide heterogenous habitats for a range of flora and fauna [5,6], and are fundamentally linked to regional biodiversity, having very high conservation value [7,8].

The ecological services and values of floodplain wetlands, particularly as wildlife habitats that support regional biodiversity, depend on their spatial and temporal environmental heterogeneity [2,9]. Floodplain biotas exhibit many adaptative mechanisms to take advantage of this heterogeneity [10–12]. Even relatively short episodes of wet and dry (days to weeks) can profoundly affect a floodplain plant community [13], which may have cascadic effects on many animals that inhabit a floodplain [14,15]. For example, in the middle to lower Yangtze floodplains, lush *Carex* meadows can develop in a newly exposed lakebed days after water level withdrawal [16]; and a study found that the wintering waterfowls changed foraging behaviors to trace newly geminated grass for maximum food intake [17].

Floodplain wetlands have long been recognized as sensitive to anthroponotic disturbances such as land reclamation and river regulation [18–20], and are globally threatened ecosystems [21,22]. For example, 80–90% of the floodplains in Europe are lost to agriculture and urban development [23]. In North America, nearly 90% of the floodplains are 'cultivated' and non-functional according to Erwin [24]. Most rivers in Australia's Murry–Darling Basin are regulated by dams and weirs, resulting in extensive wetland decline and degradation [25,26]. The loss of floodplain wetlands in large Asian river basins, such as the Yangtze [27], the Mekong [28], and the Ganges [29], is also alarming and still proceeds at a high rate. In the context of accelerating global warming, continuously shrinking floodplains will be inevitable without effective management strategies [30].

Human disruptions to hydrological regimes, such as dam operations on the river channel and embankments within the floodplain, can substantially affect floodplain vegetation succession and the distribution pattern of vegetation patches [31–33]. In most cases, the flow regulation reduces the hydrological variation in floodplain wetlands, which can lead to vegetation encroachment on the floodplain, enabling the expansion of invasive vegetation communities with low species diversity, such as *Phragmites* monoculture [34–36]. Changes in the spatial pattern of vegetation communities aggravate the decline of the ecosystem functions of floodplains through habitat fragmentation and degradation [37], ultimately leading to the loss of regional biodiversity. To mitigate the detrimental impacts of anthropogenic activities, restoration measures are practiced worldwide, aiming to re-establish fundamental hydrological parameters, such as the magnitude, frequency, duration, timing, and rate of change in river flows, that drive ecosystem functions [38]. Quantitative analyses of the relationships between flow regime and distribution dynamics of a vegetation community are necessary to understand the interaction between physical and biological processes for effective ecological restoration [39]. However, these interactive mechanisms are difficult to quantify due to the inherent complexity of vegetation dynamics and of the numerous interactions and feedbacks among different processes, such as erosion and sedimentation, vegetation recruitment and colonization [40].

Extensive floodplains occur in the middle to lower Yangtze River [41,42], supporting regional and global biodiversity [43]. Recently, many studies have provided multiple lines of evidence to suggest that the accelerating loss of floodplain functions in the region are due to economic development and climatic change [44–46], prompting enormous conservation efforts to improve or restore floodplains and their associated aquatic habitats [47]. One priority is to re-establish the key elements of the flow regime that sustains the diverse wetland types [18] which support the variety of biota depending on floodplains in their life cycles [10–12], including fish [48], waterbirds [16] and others (e.g., mammals, reptiles and amphibians) [43,49]. In this context, knowledge of the quantitative relationships between flow regime and vegetation dynamics, such as how inundation timing and duration shape the pattern and condition of vegetation mosaic [33], is pressingly needed.

Spatiotemporal analysis of floodplain vegetation cover using a time series of satellite images is approved as cost-effective for wetland monitoring [50], especially for assessing the impacts of flow regulation on floodplain ecosystems [51,52], evaluating restoration projects, and inferring future changes [53–55]. Together with flow regime variables calculated from in situ hydrological gauge records and climate observations, it is possible to determine the driving factors of observed changes [56], providing scientific insights to design effective restoration strategies [38].

Many previous studies have mapped wetland vegetation cover changes in Dongting Lake [57–60]. However, these maps have only limited usability in quantifying the relationship between flow regime and wetland habitat dynamics due to the constraints of either spatial and/or temporal resolution, or insufficient number of years of data. In this study, we aimed to identify the key flow regime parameters that drive the temporal variation of the four major wetland types (i.e., *Carex* meadows, reed marshes, mudflats, and shallow waters) in East Dongting Lake, a Ramsar site and one the most prominent floodplains in the Yangtze Basin (Figure 1). Our approach involved creating a 34-year time series (1988–2021) of wetland maps using 383 Landsat images. With the time series of yearly habitat types, we then investigated how flow regime parameters affected the interannual variations of habitat using generalized addition modelling (GAM) [61]. Finally, the loss and gain of each wetland habitat during the study period was calculated at the pixel level by comparing the habitat distribution in 1988 and 2021, and the dominant signals of change for each class were identified [62,63]. This transition matrix analysis is of particular interest to restoration planning and practice as different habitats provide distinct ecological functions, for example, *Carex* meadows and mudflats are the main foraging ground for wintering geese [17], shallow waters are a key habitat of wintering swans and storks [41], and reed swamps provide roosting and nesting sites for colonial herons, glebes and egrets [64,65], but are avoided by many migratory waterbirds. Our specific research hypotheses were: (i) hydrological regime parameters act on habitat types differentially with less effect on perennial reed beds due to their persistence; and (ii) the long-term expansion of reedbed causes the variation of other habitats, especially *Carex* meadows.

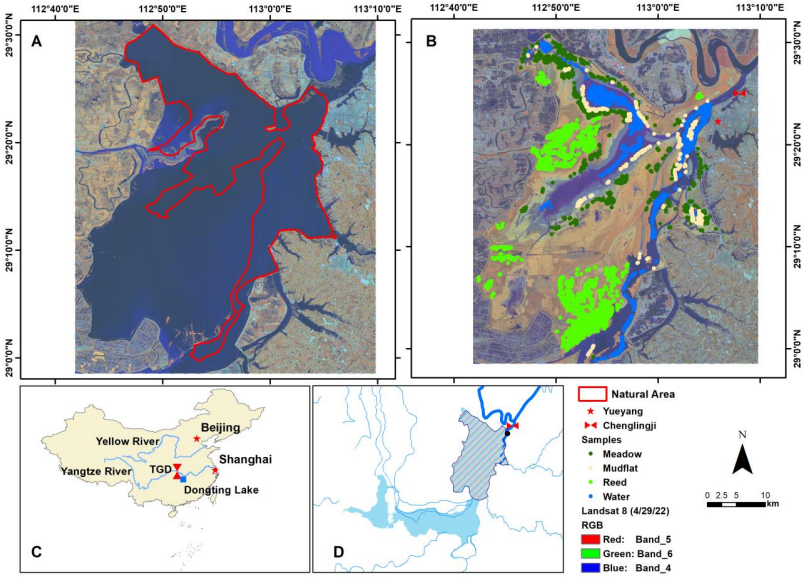

Figure 1. Landsat images show the extent of East Dongting Lake in wet ((**A**), 3 August 2022) and dry ((**B**), 29 April 2022) seasons. The stratified random samples of four major habitats were drawn from the overlaps of two habitat maps (1993 and 2010). (**C**) Map showing the location of Dongting Lake in China and its spatial relation with the Yangtze and the Three Gorges Dam (TGD). (**D**) Map showing the study area (shaded East Dongting Lake) situated in the lower section of Dongting Lake, and the thick blue line is the Yangtze River.

2. Materials and Methods

2.1. Study Site

Dongting Lake (28°30′N–30°20′N, 111°40′E–113°10′E, Figure 1) is one of most prominent freshwater lakes in the middle to lower Yangtze Basin, and is renowned for its importance for regional biodiversity [43]. The lake is divided geographically and administratively into three sections: East Dongting Lake, South Dongting Lake, and West Dongting Lake, which are connected by main river channels. This study focused on the largest section, East Dongting Lake (hereafter referred to as EDT).

Influenced by the prevailing subtropic monsoon climate, EDT has distinct wet and dry seasons with an annual water level fluctuation of 12–14 m [57]. During the wet season (April to September), the water level at Chenglingji hydrological station (Figure 1) reaches a maximum level of up to 36 m, and the entire lake virtually becomes a single water body. During the dry season of October to March, the lake water level decreases to a minimum of ~19 m. With water levels receded, a vast lakebed is exposed, and *Carex* wet meadows develop rapidly, colonizing a large part of the lake [27]. The lake landscape is dominated by connected and disconnected vegetated mosaics separated by mudflats and shallow waters, providing wintering grounds for hundreds and thousands of migratory waterbirds [16]. However, this spatial heterogeneity that maintains the conservation function is at risk due to the de-coupling of the river–lake relationship [18], calling for effective restoration strategies.

2.2. Data Sources and Preparation

Wetland habitat mapping involves four major steps (Figure 2): extracting Landsat images and computing surface reflectance-derived spectral indices; preparing sampling points; building and verifying random forest models; and prediction.

2.3. Habitat Type

To confirm that the samples could be used to model habitat extent and distribution under all hydrological conditions, we selected two maps: the 1993 map representing the dry condition (mean January water level at Chenglingji was 20.05 m), and the 2013 map representing the wet condition (mean January water level at Chenglingji was 22.18 m). With these two maps, we produced a new map where the habitat was the same in both years, through raster overlaying. Using stratified random sampling of the new map, we produced a total of 4090 samples, representing *Carex* meadow (628), mudflat (336), reedbed (1567), and open water (1559).

2.4. Predictor Variables and Pre-Processing

As the study area is located in a humid subtropic zone with a monsoon climate, cloud contamination is an issue limiting the availability of quality space-borne optical imagery for land cover mapping [66], especially for investigating habitat dynamics using time series data [67]. Using a benign 15% cloud cover threshold, there were only 241 images for the study period, and there were large gaps for many years. However, as cloud cover is calculated for the entire scene in the USGS system, applying a threshold could exclude many quality images of the study area, which covered only a proportion of the theme. For example, the image for 1 April 2004 had 60% cloud cover, but the percentage for the study area was only a negligible 1.22, and of good quality for habitat mapping (Figure A1).

To minimize the gaps in the time series, we downloaded all Landsat images (Level 2, Collection 2, Tier 1, a total of 722) for the study period (January 1988 to March 2022) using the Google Earth Engine platform. Using the pixel quality band (i.e., band 18, USGS, 2021 and 2022), we masked out all cloud and cloud shadow pixels, and recalculated the cloud cover for the study area. Images with cloud cover of less than 15% were selected for further processing (Figure 2).

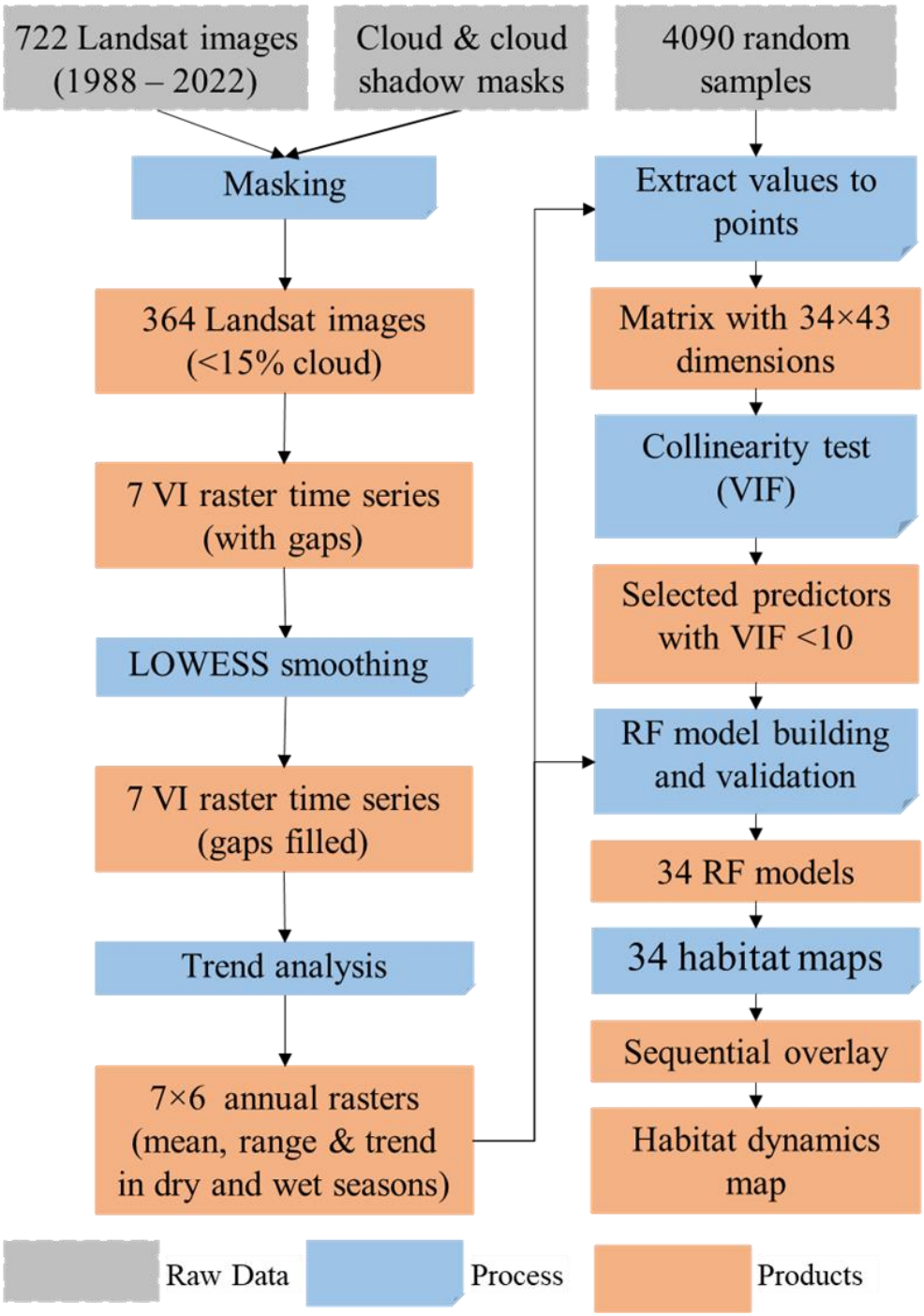

Figure 2. Flowchart illustrating wetland habitat mapping using Landsat image time series. VI = vegetation index, VIF = variable inflation factor; and RF = random forest.

Many Landsat-based spectral indices have been developed [68], and the list is increasing [69]. Considering the distinct seasonal dynamics of the habitats (Figure 1), we selected vegetation indices that are more sensitive to vegetation phenology (Table 1). Further, the bare soil index (BSI) and normalized difference water index (NDWI) were included to maximize the differentiation of mudflat and water from vegetated areas.

Table 1. Spectral indices for random forest classifier and their respective characteristics.

Name	Relevance	Formula	Reference
NDVI (normalized difference vegetation index)	NDVI measures photosynthetically active biomass in plants. It is the most highly used index to monitor plant development dynamics.	$\frac{NIR-Red}{NIR+RED}$	[70]
NDWI (normalized difference water index)	NDWI detects open water features.	$\frac{Green-NIR}{Green+NIR}$	[71]
PSRI (plant senescence reflectance index)	PSRI is sensitive to the ratio of carotenoids to chlorophyll in plants, indicating the process of vegetation senescence.	$\frac{Red-Green}{NIR}$	[72]
SAVI (soil adjusted vegetation index)	SAVI is used to mitigate the impact of soil brightness to correct NDVI in areas where vegetative cover is low.	$\frac{NIR-Red}{(NIR+RED+0.5)\times 1.5}$	[73]
GNDVI (green normalized difference vegetation index)	GNDVI is a modification of NDVI to detect wilted or aging plants and to measure nitrogen content in leaves. It is suitable to monitor vegetation with dense canopies or at different maturity stages.	$\frac{NIR-Green}{NIR+Green}$	[74]
BSI (bare soil index)	BSI is used to differentiate bare soil and other land cover types. Due to the high contrast between bare soil and vegetation, BSI provides a continuum ranging from high vegetation cover to exposed soil.	$\frac{(Red+SWIR2)-(NIR+Blue)}{(Red+SWIR2)+(NIR+Blue}$	[75]
NDPI (normalized difference phenology index)	NDPI improves the spring greening-up phenology monitoring capacity in snow-contaminated or low vegetation cover areas.	$\frac{NIR-(0.74\times Red+0.26\times SWIR1)}{NIR+(0.74\times Red+0.26\times SWIR1)}$	[76]

We used the *spline* function in R (R Development Core Team 2019) to impute the permanent gaps in the time series of the above mentioned seven indices. The method by Fritsch and Carlson (1980) [77] was adopted to fit a piecewise monotonic cubic function for each index, which was then used to predict the missing data in the time series.

Six yearly statistics were derived from the filled raster time series: mean, range (max–min), and trend for both wet and dry season. The wet season included the calendar months of April to October (seven months) and the dry season from November to March next year (five months). For computing convenience, i.e., the calculations of yearly statistics of VI in wet and dry phases, we shifted the time series back by three months, so that the wet season was January to May, and the dry season was June to December. The trend was computed as the slope of the linear regression between the index value (y) and day of the year (x).

2.5. Random Forest Models for Wetland Habitat Classification

We used the random forest (RF) approach [78] to map the yearly distribution of the four habitat types. RF is a robust supervised machine learning classifier widely used in land cover and land use mapping [79,80]. It is among the top machine learning algorithms to discriminate both inland [81] and coastal wetlands [82,83]. The main advantages of RF include: (1) the classifier can effectively handle high data dimensionality and multicollinearity [80], which is a common issue in environmental data; (2) its algorithm is insensitive to overfitting; and (3) the computing cost is relatively low while performing comparably to the more computational demanding approaches such as convolutional neural networks [84,85].

Although RF and machine learning techniques in general are relatively robust to multicollinearity of predictor variables [86], highly correlated predictors could render lower model accuracy [87]. Therefore, we performed a VIF (variable inflation factor) test, and a VIF greater than 10 was excluded from model fitting [88].

The dataset was split into training (75%) and testing (25%) subsets using stratified random sampling. With the training dataset, the repeated (five times) 10-fold cross-validation

procedure was used to fine tune the model to optimize its performance. To avoid overfit and increase prediction power, we used the *train* function in the R package "Caret" [89] to find the best model parameters. We defined a search grid with the two most important parameters (mtry—the number of variables that is randomly selected at each split; and ntree—the number of branches that will grow after each split) [90]. All other parameters such as the sampling theme and the minimal node size were kept as default. Using the testing dataset, we calculated the overall, producer, and user accuracy (OA, PA, and UA, respectively) of wetland classifications. We also evaluated the model performance with the Cohen's kappa statistic, which considers the expected error rate. While kappa = 1 indicates prefect model prediction, kappa = 0 is interpreted as no agreement between observations and predictions.

2.6. Wetland Habitat Dynamics during 1989–2021

To explore the change in the extent and distribution of wetland habitats, we conducted a grid-by-grid comparison between habitat maps of the first (1988) and the last (2021) years: the two habitat maps were overlaid to produce a transition matrix of the four habitat types. The changes in habitat types were quantified in terms of gross gains, gross losses, and persistence, as well as net and swap changes. The swap change refers to gross loss of type in one area with a gross gain of the same type in another location, or vice versa [63]. With the class transition matrix, we further computed the loss-to-persistence ratio (i.e., loss/persistence) and gain-to-persistence ratio (i.e., gain/persistence) to assess the tendency of each wetland type to lose to, and gain from, other types, which was an approach developed by Braimoh (2006) [62].

2.7. Drivers of Wetland Vegetation Dynamics

The hydrological regimes were quantified with nine variables: date of rising (DOYR, day of year—DOY), rate of water level rising (ROR, m/day), date of withdrawal (DOYW, DOY), duration of low water season (DOD, days), rate of water level withdrawal (ROW, m/day), mean water level during high water season (MHH, m), mean water level during low water season (MHL, m), peak water level (m), and lowest water level (m). These hydrological metrics characterize the magnitude, timing, duration, and rate of change constituting the key flow components that regulate riverine ecosystems [91]. The raw daily water level records series (1988–2021) at Chenglingji was first smoothed using singular spectrum analysis (SSA) [92]. The hydrological regime variables were then derived from the smoothed water level curve. Total rainfall and mean temperature during dry season were calculated from climate records from the weather station at Yueyang.

We investigated the effects of hydrological regime and climate on habitat dynamics using generalized additive mixed models (GAMM) implemented in the R (http://cran.r-project.org; last visited 16 June 2022) package 'mgcv' [93], which accounts for complex nonlinear patterns [61]. To reduce the confounding effects of human activities, such as plantation and winter cropping, we restricted the investigation to the "natural area" (Figure 2), which is relatively free of levees and weirs, by manually inspecting the aerial photos. For each year, the predicted distributions of the habitats within this area were extracted. The GAMM modelled the proportions of meadow, mudflat and reed in response to hydrological regimes and climatic variables.

Instead of fitting three separate GAM, we included habitat type (Type) as a random effect in the model formula to investigate the habitat-specific effect of predictor variables:

$$\text{gam (Y = Type + Year + X1 + X2 + s(Year, by = Type)+ s(X1, by = Type) + s(X2, by = Type)}$$

where Y is the area percentage of each habitat type, Type is factor variable of the three habitat types, Year is the sampling year, and X1 and X2 are independent variables (i.e., hydrology or climate). We included Year in the model to account for overall trends of habitat and the autocorrelation of the time series data.

As the response variables are proportions (i.e., bounded by 0 and 1), we specified a beta distribution with a logit-link function. This link function also takes into account the observed and unobserved heterogeneity in the data [94]. Due to the small sample size (i.e., 34 years of data), we limited the number of covariates to three to keep the risk of overfitting low. Covariate selection was based on the generalized likelihood ratio test (GLRT) [61]. However, in cases of non-significant test ($p > 0.05$, models are not significantly different), both models were selected and reported on. Moreover, when fitting the GAMM, we added an additional penalty (i.e., the double penalty approach) to remove redundant covariates [95]. The additional penalty affects the functions in the null space of the original penalty. Thus, if all the smoothing parameters for a variable tended to infinity, this variable would be excluded from the final model [95]. Finally, we checked the model residuals for normality by visually inspecting the residual plots and autocorrelation using the Durbin–Watson test [96].

3. Results

3.1. Model Accuracy Assessment

All RF models had high overall accuracy and could be considered as "almost perfect" based on the kappa statistics [97] as the kappa coefficient of agreement was greater than 0.90 for all models. The lowest kappa (0.93) belonged to the 2002 model, and the model for 2014 had the highest kappa of 0.98 (Figure 3). Moreover, as the overall accuracy and kappa coefficient of agreement were comparable for training and testing, there was little evidence of overfitting.

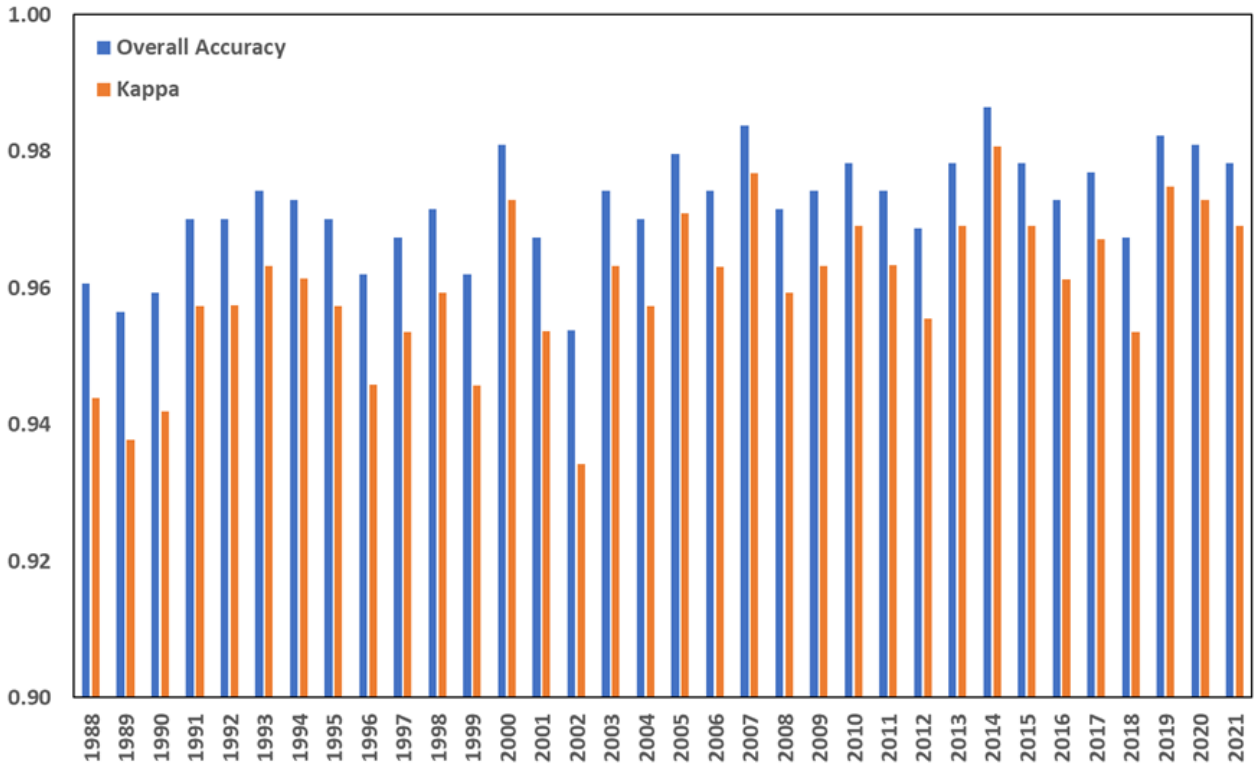

Figure 3. Testing overall accuracy (mean = 0.98) and kappa (mean = 0.97) of the 34 wetland habitat classification models.

At the class level, accuracies were also high (Figure 4). Overall, mudflat had the lowest producer's and user's accuracy. The variance for mudflat was also the highest (i.e., the largest standard deviation, Figure 4), and RF had a tendency to underestimate mudflats. The misclassification mainly came from two sources. The first was the confusion between water and mudflat, and to a lesser degree, between mudflat and meadow (Table 1). Reed and water had comparably high accuracy for both PA and UA (Figure 4), and PA and UA

were 100% in many cases. The discrimination capacity for meadow was in the middle (Figure 4), and most of the errors were from the confusion between meadow and mudflat (Table 2). The high accuracy ensured the trustworthy habitat mapping of further analyses.

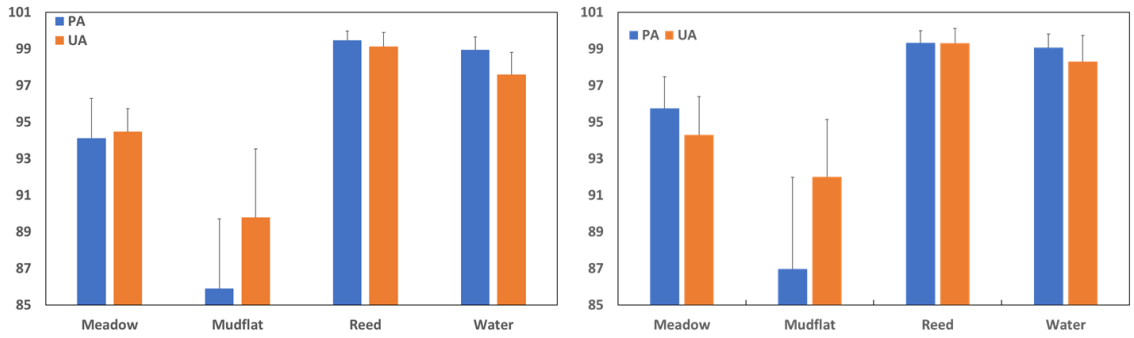

Figure 4. Producer's accuracy (PA) and user's accuracy (UA) of the four classes for model training (**left**) and testing (**right**). Columns are the mean of 34 RF models, and bars are the standard deviation.

Table 2. The testing confusion matrix of the worst model for mudflat (year 1989), with producer's accuracy (PA) and user's accuracy (UA).

Class	Meadow	Mudflat	Reed	Water	Sum	PA (%)
Meadow	147	8	0	0	155	94.8
Mudflat	8	55	0	0	63	87.3
Reed	0	0	299	0	299	100
Water	2	14	0	203	219	92.7
Sum	157	77	299	203	736	
UA (%)	93.6	71.4	100	100		95.7 (OA)

3.2. Spatial Extent of Habitat Transitions

The spatial extent of habitat loss, gain, and persistence during the study period of 34 years is presented in Figure 5. Overall, nearly 70% of the habitats mapped in 1988 remained the same in 2021 (Figure 5). However, the expansion of reed was extensive in some places, and localized erosion and lakebed build-up was also identified.

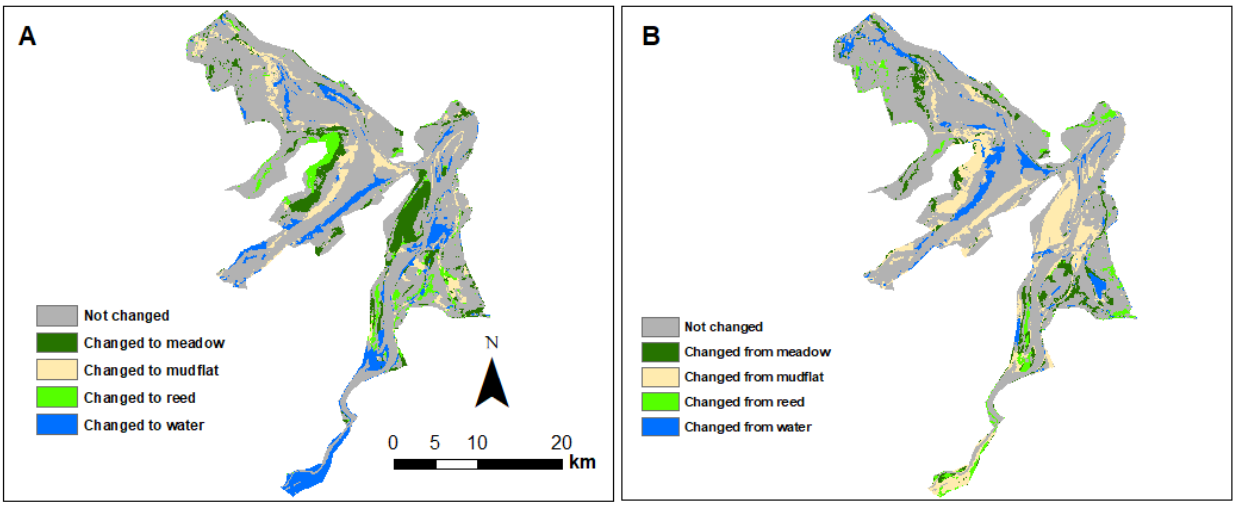

Figure 5. Maps of habitat transition showing that most of the habitat (nearly 70%) remained the same during the study period of 1988–2022. Map (**A**) shows the locations of reed and meadow expansion, as well as the places of erosion (i.e., becoming water). Map (**B**) shows that a large part of the original mudflat was lost, and the places of lakebed build-up (i.e., water replaced by other habitats).

Transitions of habitat from one type to other types over the 34 year study period, including gains, losses, persistence, total changes, and swaps, are summarized in Table 3. The spatial extent of habitat loss, gain, and persistence during the study period of 34 years is presented in Figure 5. At lake scale, the total changes were dominated by mudflat (TC was 22.38%, 15.88%, 13.68% and 5.74%, for mudflat, meadow, water, and reed, respectively, Table 3). Mudflat, meadow and water had comparable swamp change, but reed had the lowest swamp change. While reed and meadow had similarly high relative persistence (84% of the land occupied by reed or meadow in 1988 remained as the same in 2021, Table 3), mudflat had the lowest relative persistence and 57% of the 15,320 ha mudflat area mapped in 1988 transferred to *Carex* meadow (4381 ha), water (3594 ha), or reedbed (748 ha) (Table 3). While reed had the least potential to change to other habitats, it also had the largest potential to gain.

Table 3. Summary of habitat transition (percentage of the total lake area) in East Dongting Lake during the period of 1988–2021. The shaded part is the transition matrix with year 1988 in columns and year 2021 in rows.

	Meadow	Mudflat	Reed	Water	Persistence	Gain	Loss	NC	SC	TC	P/T	G/P	L/P
Meadow	29.64	8.17	0.98	0.96	29.64	10.11	5.76	4.35	11.53	15.88	0.84	0.34	0.19
Mudflat	1.56	12.30	0.24	4.31	12.30	6.12	16.27	−10.15	12.23	22.38	0.43	0.50	1.32
Reed	2.81	1.39	7.10	0.23	7.10	4.43	1.31	3.12	2.62	5.74	0.84	0.62	0.18
Water	1.39	6.70	0.09	22.12	22.12	8.18	5.50	2.68	11.00	13.68	0.80	0.37	0.25

NC = net change, SC = swap change, TC = total change, P/T = persistence/total area in 1988, G/P = gain/persistence, L/P = loss/persistence. Lake area = 53,632 ha.

Over the 34 years, mudflat was the only habitat that suffered net loss (5444 ha). A total of 8723 ha of the original mudflat was lost to meadow (4381 ha), water (3594 ha), and reed (748 ha). Although reed was the smallest habitat type in Dongting Lake, it had the most relative gain (the total area increased 53% from 4157 ha to 6187 ha, Table 3). Most of this gain resulted from expansion into meadow and mudflat. More than three thousand hectares of the original meadow was lost, mostly due to the encroachment of reed (1507 ha). However, this loss was overly compensated by expansion into mudflat (4381 ha).

3.3. Drivers of Vegetation Development in East Dongting Lake

Two models fitted the data equally well (p = 0.49, GLRT test): one had DOD (duration of dry season, hereafter referred to as duration model), and the other had DOYD (dates of water level withdrawal, hereafter referred to as date model) as covariate (Table 4). Although the date model had slightly lower AIC (Akaike information criterion) than the duration model, both models explained the majority of the deviance (98.6%) in the data and had a high adjusted R^2 of 0.984. The two models produced similar response curves for year and rainfall (Table 4, Figures 6 and 7). Note that the two flow regime variables (DOD and DOYD) were significantly negatively correlated (Pearson's correlation coefficient = −0.69).

Despite the overall effects of year and rainfall not being significant, the response curves were distinct for the three habitat types. The meadow area did not vary significantly over the study period (i.e., both models estimated that the effect of year was zero). The reed area increased almost linearly over the period of 1988–2021, while the mudflat area was relatively constant before year 1998, after which it decreased almost linearly (Figure 6).

Both duration of dry season and date of water level withdrawal had no effect on the reed area (p = 0.465 and 0.302 for the DOS and DOYD, respectively, Table 4 and Figure 7). While the meadow area was positively related to the duration of dry season, it decreased with the date of water level withdrawal, and the effects were significant and more or less constant (i.e., straight response curves, Figure 7). The effect of the two hydrological regime variables on the mudflat area was highly nonlinear. The mudflat area decreased significantly with the day of the year when the water level started to decline. However, if the water level withdrawal began after late September (i.e., DOY > 270), the effect was

positive but small (Figure 8). Mudflat had a similar nonlinear response curve to the duration of dry season (Figure 8), but the effect was insignificant (p = 0.068, Table 4).

Table 4. Summary of the two fitted GAMM for wetland habitat variation in East Dongting Lake during 1988–2021.

	Duration Model					Date Model			
Parametric Term	**Est.**	**SE**	**z-Value**	***p* ***		**Est.**	**SE**	**z-Value**	***p***
Intercept	−1.264	0.453	−2.793	**0.005**	Intercept	−2.005	0.491	−4.088	**0.000**
DOD	−0.001	0.001	−2.185	**0.029**	DOYD	0.002	0.001	2.464	**0.014**
Smooth term	**edf**	**Ref.df**	**Chi.sq**	***p***		**edf**	**Ref.df**	**Chi.sq**	***p***
s(Year): Meadow #	0.000	9	0.000	0.690	s(Year): Meadow	0.000	9	0.000	0.730
s(Year): Mudflat	2.140	9	58.778	**0.000**	s(Year): Mudflat	2.110	9	55.954	**0.000**
s(Year): Reed	0.844	9	6.633	**0.010**	s(Year): Reed	0.857	9	7.368	**0.008**
s(Hab)	1.999	2	4895.312	**0.000**	s(Hab)	1.999	2	4859.347	**0.000**
s(DOD): Meadow	1.759	9	11.336	**0.000**	s(DOYD): Meadow	0.915	9	11.851	**0.000**
s(DOD): Mudflat	1.342	9	3.263	0.068	s(DOYD): Mudflat	1.774	9	7.512	**0.010**
s(DOD): Reed	0.000	9	0.000	0.465	s(DOYD): Reed	0.000	9	0.000	0.302
s(Rain): Meadow	1.161	9	2.514	0.108	s(Rain): Meadow	0.592	9	0.809	0.239
s(Rain): Mudflat	1.795	9	17.702	**0.000**	s(Rain): Mudflat	1.743	9	16.902	**0.000**
s(Rain): Reed	2.184	9	15.608	**0.001**	s(Rain): Reed	1.993	9	10.801	**0.004**
R^2 (adj)	0.984				R^2 (adj)	0.984			

edf = effective degree of freedom; Ref.df = reference degree of freedom; Chi.sq = Chi square. DOD = duration of dry season (days); DOYD = date of water level withdrawal (day of year); and Rain = total precipitation in winter. # s = smoothing term; * Bold indicated significant, and p = 0.000 means < 0.00001.

The effects of dry season rainfall on meadow were small and insignificant while its effects on mudflat and reed were nonlinear and significant (Table 4 and Figure 8). The mudflat area decreased with the increase in dry season rainfall, although the decreasing slope was small at the two extreme ends (i.e., too dry or too wet, Figure 8). The reed area increased with rainfall until ~300 mm, after which the effect of rainfall was negative (Figure 8).

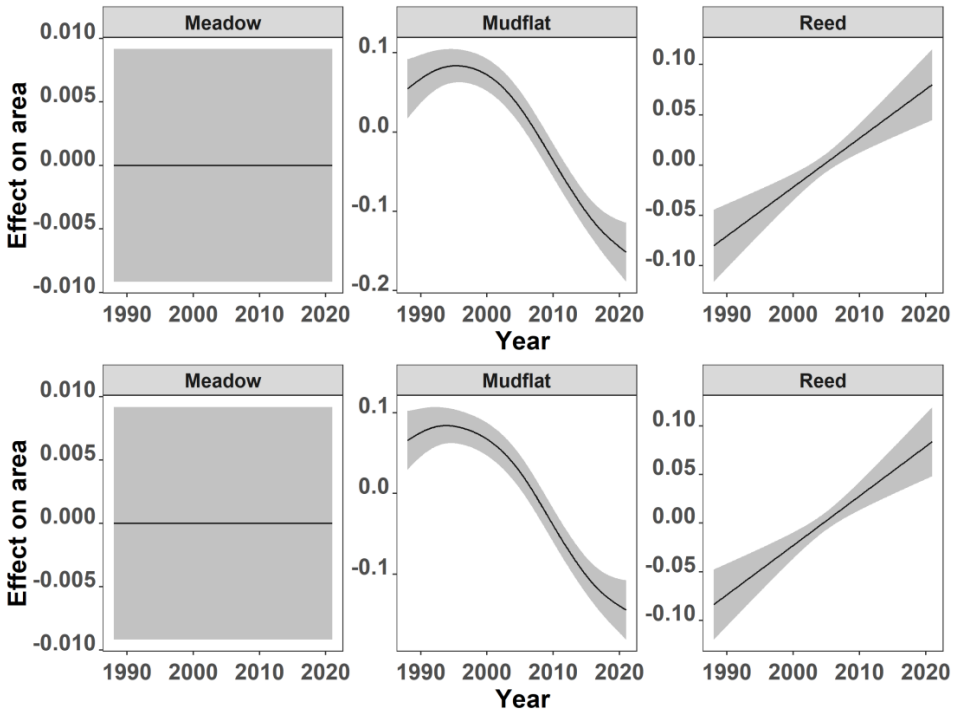

Figure 6. Modelled response curves to year from the duration model (upper panel) and date model (lower panel). Black lines are the estimate, and the grey shaded areas are 95% confident intervals. The Y-axis is the modelled partial response of habitat area to year. Note the zero effect on meadow (the modelled partial effect is a flat line).

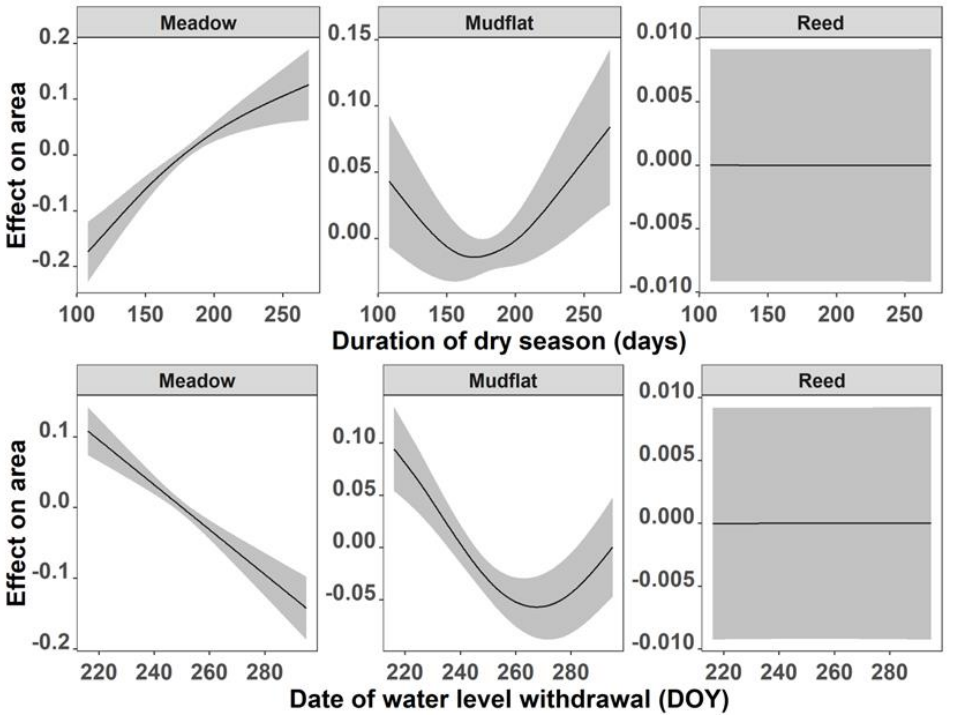

Figure 7. Modelled response curves to duration of dry season (upper panel) and date of water level withdrawal (lower panel). Black lines are the estimate and the grey shaded areas are 95% confident intervals. The Y-axis is the modelled partial response of habitat area to date of water level withdrawal. Note that the modelled partial effect of both DOD and DOYD on reed is a flat line.

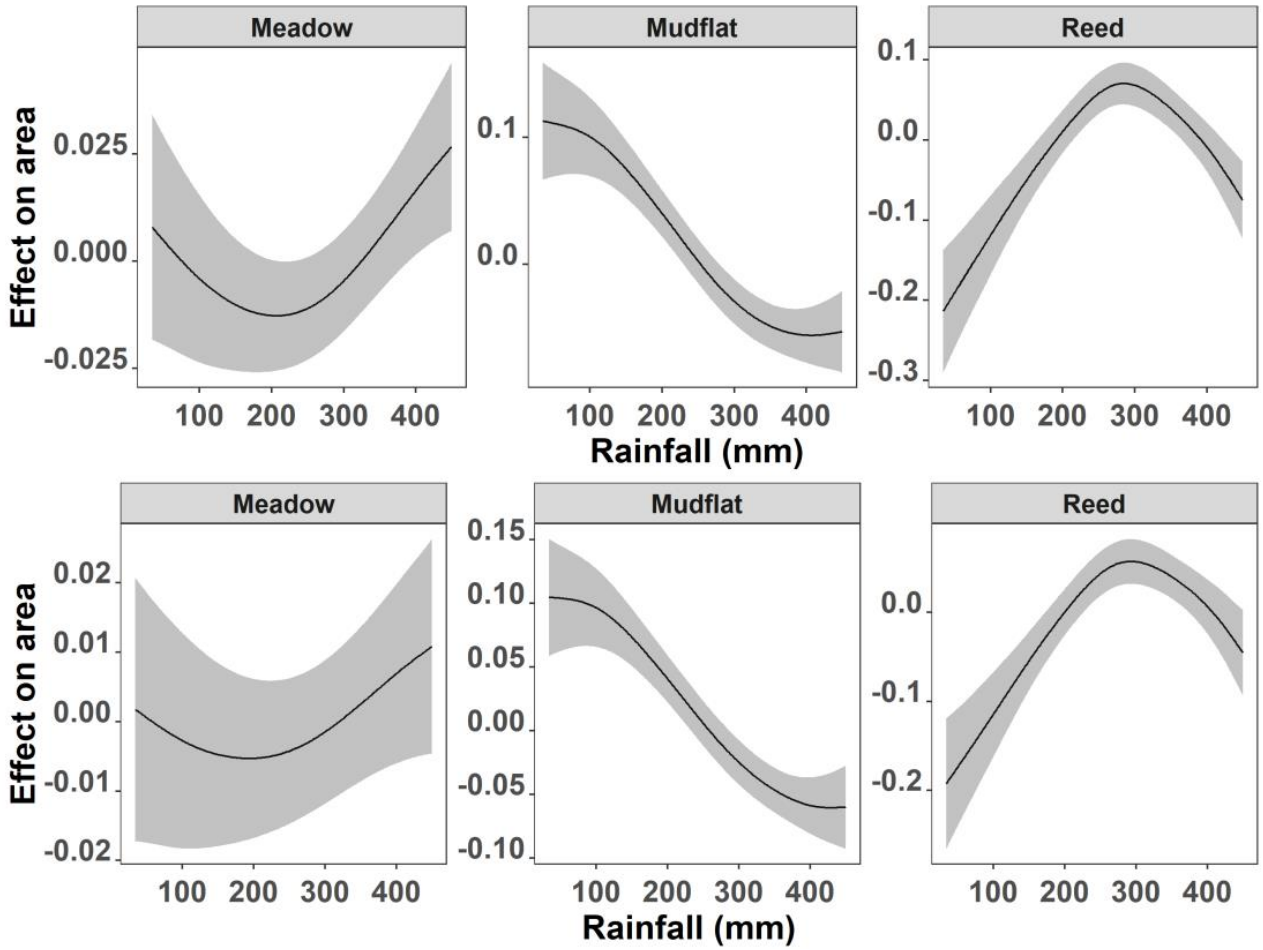

Figure 8. Modelled response curves to dry season rainfall from the duration model (upper panel) and date model (lower panel). Black lines are the estimate and the grey shaded areas are 95% confident intervals. Note that the effect on meadow is small and insignificant (Table 4).

4. Discussion

4.1. Overall Evaluation of Mapping Approach

Medium resolution satellite imagery, such as the 30 m Landsat TM, ETM+, or OLI, is often preferred for mapping wetland vegetation at large scale [98]. Although high performance classification can be achieved using a single date satellite image [57,99], multitemporal data that capture the vegetation phenology are often more robust [100, 101] due to the highly dynamic nature of the floodplain landscape [2,13]. This study retrospectively created a long-term time series (1988–2021) of yearly wetland vegetation cover in the EDT floodplain using multitemporal Landsat images. Our approach had three main advantages that contributed to the superior classification power (Figures 3 and 4) despite the slight underestimation of mudflats and overestimation of water.

First, we maximized the number of available images used in vegetation indices computing. The study area is located in a subtropical monsoon region; therefore, high quality satellite images are limited if selected by the percentage of cloud cover over the whole scene [51,57,99,101]. A previous study using an image fusion of Landsat and MODIS (moderate resolution imaging spectroradiometer) data to address this issue achieved acceptable performance [67]. Recalculation of cloud cover with pixel quality assessment (band 18) greatly increased the number of useable images (i.e., a total of 364). The high frequency image collection justified the further procedures to extract the vegetation phenology for classification.

Second, lack of ground-truth samples is an obvious drawback for mapping historical vegetation distribution retrospectively. Many studies have used historical high-resolution satellite and/or aerial photos available from Google Earth or other platforms (such as Nearmap Australia, website accessed on 29 March 2022, https://www.nearmap.com/au/en) to compile a testing dataset and model training [101,102]. Here, we overlaid two historical vegetation maps representing dry and wet conditions more than 10 years apart to create stratified random samples. The approaches captured the characteristic wetland types for the whole study period and guaranteed the ability of the samples for the entire study period.

Finally, we extracted the essential phenological variables for classification. The four wetland covers had distinct signatures in terms of the 42 vegetation indices (Figure 2). For example, the NDVI values for reedbed increased in wet but decreased in the dry season, and *Carex* meadows had the opposite trend [27]. The combination of these phenological variables resulted in accurate and precise classification. Nevertheless, there were uncertainties between mudflat and water, both of which had very low vegetation indices values and no clear trends in wet or dry seasons. The inclusion of image texture features [101] might improve the discrimination of the two classes.

4.2. Drivers of Wetland Vegetation Dynamics

The mapping of the floodplain wetland types was not a primary objective of this study. The long-term time series of yearly maps was created to investigate how wetland habitats respond to river flow variation for designing effective restoration.

Overall, the duration of the low water season and date of water level withdrawal were found to be the primary drivers of wetland habitat dynamics. Many studies demonstrate that vegetation patterns in floodplains are driven by the hydroperiod, i.e., the duration and temporal pattern of inundation [57,58,91]. Spatial variations in the hydroperiod, which can result from minor differences in elevation (i.e., microtopographic pattern), often produce dramatic differences in vegetation across floodplains [103]. However, the effects of all other tested flow regime variables, such as the rate of water level withdrawal, mean water levels during high and low water seasons, and the lowest water level, were insignificant. The results were largely consistent with our previous findings [57], which found that the development of *Carex* meadow in the EDT floodplain was positively related to the date of water level withdrawal. However, these findings were at odds with Peng et al. [101], who reported the close correlations between the size of reedbed and *Carex* meadow area and water level at different seasons. The main reason for this disagreement might be the different focus areas. To reduce the confounding impacts of human activities on the floodplain, we excluded areas with reed plantation and winter cropping (Figure 2), whereas Peng et al. [101] investigated the entire lake.

4.2.1. Reedbed Is Highly Persistent and Has Rapidly Expanded during the Study Period

Throughout the study period, the majority of original reedbed patches remained (Table 3 and Figure 5), showing the greatest persistence to changes in flow regime (Figure 8). On the other hand, the total reedbed area increased 2337 ha (or 62%) by encroaching into *Carex* meadows (1507 ha) and mudflats (748 ha) over the 34 years. Expansion of reedbeds is a worldwide phenomenon that has biodiversity concern [104]. The gradual encroachment of reedbeds (Figure 6) into *Carex* meadows and mudflats will be a great threat to the hundreds and thousands of waterbirds such as geese and swans wintering in EDT [16,17].

Surprisingly, none of the flow regime variables had significant effects on the expansion of reedbed area (Figures 6 and 7, Table 4). The lack of relationship with flow regime could be linked with the life form of *Phragmites*, which is a tall (up to 4 m) rhizomatous grass, enabling it to survive the maximum water depth at areas currently occupied by *Carex* meadows and mudflats. Moreover, *Phragmites* seeds spread copiously and clonally by a vigorous system of rhizomes and stolons [105], therefore, can proliferate other habitats through both clonal and sexual reproduction once recruited and established in

wetland [106]. Other broader scale factors, such as the increase in winter rainfall associated with climate change [107], and the elevated atmospheric CO_2 level (108), might be responsible for the continuous spread of this cosmopolitan species.

4.2.2. Carex Meadow Has No Trend and Fluctuates with the Changes in Flow Regime

Although the mapped area of *Carex* meadow in 2021 was greater than that in 1988 (Table 3), the total area of *Carex* meadow varied greatly between years and showed no trend (Figure 6), which was consistent with the findings of a previous study [101]. The interannual variations of *Carex* meadow area in EDT were the balanced outcome of loss to reedbed and gain from mudflat. While loss to reedbed was permanent (i.e., once an area was replaced by reed, it remained as reed), the gain from mudflat was somehow transient (i.e., there were many pixels switching between *Carex* meadow and mudflat). In addition, the switching between *Carex* meadow and mudflat contributed more to the year-to-year changes in total *Carex* meadow area, and the majority of pixels that had high tendency to swap were located at the transient zone between the two habitats (Figure 5). A previous study found that the wintering geese preferred to forage in this transient zone [16], indicating its conservation importance.

The results of GAM indicated that the *Carex* meadow area increased with the duration of the dry season and decreased with the day of the year when the water level started to withdraw (Figure 8), which was consistent with both field observation and lab gemination experiment [108]. The importance of the water level withdrawal date might be related to the temperature requirement of the gemination of the species. In the middle Yangtze region, the rhizomes of the tufted perennial grass *Carex* spp. generally cannot regerminate when the air temperature is below 6 °C [109]. As the DOY of the water level withdrawal increases, the air temperature decreases, reducing the colonization of *Carex* meadows.

4.2.3. Mudflat Is the Most Vulnerable Habitat

Being the only habitat type to show significant decrease during the 34-year period (Figure 6), mudflat had the lowest persistence/total value (Table 3), and was vulnerable to being replaced by other habitat types. By inspecting the yearly habitat maps, three processes of loss were identified: (1) permanent replacement by reedbed; (2) irreversible loss to water (i.e., erosion); and (3) transitional swapping with *Carex* meadow. Moreover, the switch to and from mudflats was not symmetrical, with a higher tendency of shifting from mudflat to *Carex* meadow, resulting in the slow advance of the transient zone towards water. The accelerated erosion might be attributed to sand mining, a serious threat identified in many river systems of the Yangtze Basin [42].

Mudflats have long been recognized as important foraging habitat for shorebirds in coastal areas [110]. However, the ecological function of mudflats in freshwater floodplains are largely overlooked; and most restoration projects focus on vegetated areas and shallow waters. Nevertheless, they are also important resting and foraging habitats for a range of wintering waterbirds in the Yangtze region [65]. Many waterbirds, such as swans and storks, prey on organisms dwelling in mudflats [111]. The loss and vulnerability of mudflat in EDT should be closely monitored.

5. Conclusions

Restoration of floodplain wetland associated with large rivers is vital for global biodiversity. Understanding how flow regime shapes wetland vegetation cover is critical for effective restoration. In this study, we built a 34 year (1988–2021) time series map of wetland habitat using Landsat imagery and machine learning algorithm. The spatiotemporal dynamics of four broad habitats were further investigated using GAMM. Our analysis revealed the constant expansion of reedbeds and shrinkage of mudflats, which might degrade the conservation function of the Ramsar wetland. The GAMM results showed that the duration of dry season and the date when the water level started to withdraw were the key flow regime parameters acting on the extent of wetland habitats. Moreover,

the responses of different wetland vegetation to flow variations were distinct. Specifically, while *Carex* meadow increased with an earlier water withdrawal and longer dry season, reedbed continuously spread out independent of flow regime.

Author Contributions: Conceptualization, L.J., L.W., Q.Z. and C.L.; data curation, L.W.; formal analysis, G.L. and L.W.; funding acquisition, W.L. and G.L.; investigation, L.J., K.H., P.L. and R.F.; methodology, L.J. and L.W.; project administration, W.L. and C.L.; software, L.W.; supervision, L.W.; validation, L.J., G.L. and C.L.; visualization, L.J. and C.L.; writing—original draft, L.J., Q.Z. and C.L.; writing—review and editing, L.W. and C.L. All authors have read and agreed to the published version of the manuscript.

Funding: This research was funded by the National Key Research and Development Program of China, grant number 2017YFC0405300; the National Natural Science Foundation of China, grant numbers U20A2089 and 41971152; and the Natural Science Foundation of Hunan Province, China, grant number 2021JJ20012.

Data Availability Statement: Data will be made available on request.

Acknowledgments: The authors thank Changjiang Water Resource Commission for providing the hydrological data, and thank the staff of the East Dongting Lake Nature Reserve Authority for their help in the field investigation.

Conflicts of Interest: The authors declare no conflict of interest.

Appendix A

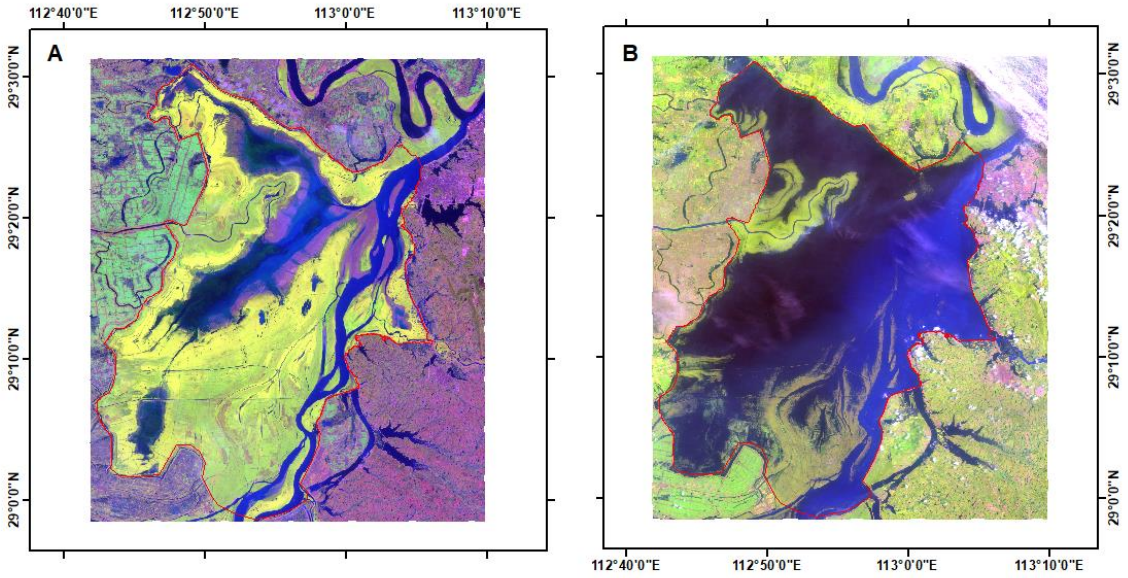

Figure A1. Landsat 5 images obtained on 1 April 2004 (**A**) and 7 July 2010 (**B**) could be excluded if applying a threshold of 25% to select quality imagery. The cloud cover is 60% and 48%, respectively, for all themes (row 40 and path 123).

References

1. Keddy, P.A.; Fraser, L.H.; Solomeshch, A.I.; Junk, W.J.; Campbell, D.R.; Arroyo, M.T.; Alho, C.J. Wet and wonderful: The world's largest wetlands are conservation priorities. *BioScience* **2009**, *59*, 39–51. [CrossRef]
2. Lewis, W.M.; Hamilton, S.K.; Lasi, M.A.; Rodríguez, M.; Saunders, J.F. Ecological Determinism on the Orinoco Floodplain: A 15-year study of the Orinoco floodplain shows that this productive and biotically diverse ecosystem is functionally less complex than it appears. Hydrographic and geomorphic controls induce a high degree of determinism in biogeochemical and biotic processes. *BioScience* **2000**, *50*, 681–692.
3. Tickner, D.; Opperman, J.J.; Abell, R.; Acreman, M.; Arthington, A.H.; Bunn, S.E.; Cooke, S.J.; Dalton, J.; Darwall, W.; Edwards, G.; et al. Bending the curve of global freshwater biodiversity loss: An emergency recovery plan. *BioScience* **2000**, *70*, 330–342. [CrossRef] [PubMed]

4. Junk, W.J.; Bayley, P.B.; Sparks, R.E. The flood pulse concept in river-floodplain systems. In *Canadian Special Publications of Fisheries and Aquatic Sciences, Proceedings of the International Large River Symposium, Honey Harbour, ON, Canada, 14–21 September 1986*; Dodge, D.P., Ed.; Department of Fisheries and Oceans: Honey Harbour, ON, Canada, 1989; Volume 106, pp. 110–127.
5. Arthington, A.H.; Godfrey, P.C.; Pearson, R.G.; Karim, F.; Wallace, J. Biodiversity values of remnant freshwater floodplain lagoons in agricultural catchments: Evidence for fish of the Wet Tropics bioregion, northern Australia. *Aquat. Conserv. Mar. Freshw. Ecosyst.* **2015**, *25*, 336–352. [CrossRef]
6. Pander, J.; Mueller, M.; Geist, J. Habitat diversity and connectivity govern the conservation value of restored aquatic floodplain habitats. *Biol. Conserv.* **2018**, *217*, 1–10. [CrossRef]
7. Olson, D.M.; Dinerstein, E. The Global 200: A representation approach to conserving the Earth's most biologically valuable ecoregions. *Conserv. Biol.* **1998**, *12*, 502–515. [CrossRef]
8. Ward, D.P.; Pettit, N.E.; Adame, M.; Douglas, M.M.; Setterfield, S.A.; Bunn, S.E. Seasonal spatial dynamics of floodplain macrophyte and periphyton abundance in the Alligator Rivers region (Kakadu) of northern Australia. *Ecohydrology* **2016**, *9*, 1675–1686. [CrossRef]
9. Wang, Y.; Jia, Y.; Guan, L.; Lu, C.; Lei, G.; Wen, L.; Liu, G. Optimizing hydrological conditions to sustain wintering waterbird populations in Poyang Lake National Natural Reserve: Implications for dam operations. *Freshw. Biol.* **2013**, *58*, 2366–2379.
10. Adis, J.; Junk, W.J. Terrestrial invertebrates inhabiting lowland river floodplains of Central Amazonia and Central Europe: A review. *Freshw. Biol.* **2002**, *47*, 711–731. [CrossRef]
11. Jackson, M.B.; Colmer, T. Response and adaptation by plants to flooding stress. *Ann. Bot.* **2005**, *96*, 501–505. [CrossRef]
12. Parolin, P. Submerged in darkness: Adaptations to prolonged submergence by woody species of the Amazonian floodplains. *Ann. Bot.* **2009**, *103*, 359–376. [CrossRef] [PubMed]
13. Thapa, R.; Thoms, M.C.; Parsons, M. The response of dryland floodplain vegetation productivity to flooding and drying. *J. Arid Environ.* **2016**, *129*, 42–55. [CrossRef]
14. Doledec, S.; Statzner, B. Theoretical habitat templets, species traits, and species richness: 548 plant and animal species in the Upper Rhône River and its floodplain. *Freshw. Biol.* **1994**, *31*, 523–538. [CrossRef]
15. Robinson, C.T.; Tockner, K.; Ward, J.V. The fauna of dynamic riverine landscapes. *Freshw. Biol.* **2002**, *47*, 661–677. [CrossRef]
16. Guan, L.; Lei, J.; Zuo, A.; Zhang, H.; Lei, G.; Wen, L. Optimizing the timing of water level recession for conservation of wintering geese in Dongting Lake, China. *Ecol. Eng.* **2016**, *88*, 90–98. [CrossRef]
17. Lei, J.; Jia, Y.; Wang, Y.; Lei, G.; Lu, C.; Saintilan, N.; Wen, L. Behavioural plasticity and trophic niche shift: How wintering geese respond to habitat alteration. *Freshw. Biol.* **2019**, *64*, 1183–1195. [CrossRef]
18. Lu, C.; Jia, Y.; Jing, L.; Zeng, Q.; Lei, J.; Zhang, S.; Lei, G.; Wen, L. Shifts in river-floodplain relationship reveal the impacts of river regulation: A case study of Dongting Lake in China. *J. Hydrol.* **2018**, *559*, 932–941. [CrossRef]
19. Nilsson, C.; Reidy, C.A.; Dynesius, M.; Revenga, C. Fragmentation and flow regulation of the world's large river systems. *Science* **2005**, *308*, 405–408. [CrossRef]
20. Tockner, K.; Pusch, M.; Borchardt, D.; Lorang, M.S. Multiple stressors in coupled river-floodplain ecosystems. *Freshw. Biol.* **2010**, *55* (Suppl. S1), 135–151. [CrossRef]
21. Dudgeon, D.; Arthington, A.H.; Gessner, M.O.; Kawabata, Z.I.; Knowler, D.J.; Lévêque, C.; Naiman, R.J.; Prieur-Richard, A.H.; Soto, D.; Stiassny, M.L.; et al. Freshwater biodiversity: Importance, threats, status and conservation challenges. *Biol. Rev.* **2006**, *81*, 163–182. [CrossRef]
22. Opperman, J.J.; Galloway, G.E.; Fargione, J.; Mount, J.F.; Richter, B.D.; Secchi, S. Sustainable floodplains through large-scale reconnection to rivers. *Science* **2009**, *326*, 1487–1488. [CrossRef] [PubMed]
23. Tockner, K.; Stanford, J.A. Riverine flood plains: Present state and future trends. *Environ. Conserv.* **2002**, *29*, 308–330. [CrossRef]
24. Erwin, K.L. Wetlands and global climate change: The role of wetland restoration in a changing world. *Wetl. Ecol. Manag.* **2009**, *17*, 71–84. [CrossRef]
25. Chen, Y.; Colloff, M.J.; Lukasiewicz, A.; Pittock, J. A trickle, not a flood: Environmental watering in the Murray–Darling Basin, Australia. *Mar. Freshw. Res.* **2020**, *72*, 601–619. [CrossRef]
26. Kingsford, R.T.; Basset, A.; Jackson, L. Wetlands: Conservation's poor cousins. *Aquat. Conserv.* **2016**, *26*, 892–916. [CrossRef]
27. Guan, L.; Wen, L.; Feng, D.; Zhang, H.; Lei, G. Delayed flood recession in central Yangtze floodplains can cause significant food shortages for wintering geese: Results of inundation experiment. *Environ. Manag.* **2014**, *54*, 1331–1341. [CrossRef] [PubMed]
28. Mahood, S.P.; Poole, C.M.; Watson, J.E.; MacKenzie, R.A.; Sharma, S.; Garnett, S.T. Agricultural intensification is causing rapid habitat change in the Tonle Sap Floodplain, Cambodia. *Wetl. Ecol. Manag.* **2020**, *28*, 713–726. [CrossRef]
29. Singh, M.; Sinha, R. Evaluating dynamic hydrological connectivity of a floodplain wetland in North Bihar, India using geostatistical methods. *Sci. Total Environ.* **2019**, *651*, 2473–2488. [CrossRef]
30. Xi, Y.; Peng, S.; Ciais, P.; Chen, Y. Future impacts of climate change on inland Ramsar wetlands. *Nat. Clim. Chang.* **2021**, *11*, 45–51. [CrossRef]
31. Benjankar, R.; Jorde, K.; Yager, E.M.; Egger, G.; Goodwin, P.; Glenn, N.F. The impact of river modification and dam operation on floodplain vegetation succession trends in the Kootenai River, USA. *Ecol. Eng.* **2012**, *46*, 88–97. [CrossRef]
32. Catford, J.A.; Downes, B.J.; Gippel, C.J.; Vesk, P.A. Flow regulation reduces native plant cover and facilitates exotic invasion in riparian wetlands. *J. Appl. Ecol.* **2011**, *48*, 432–442. [CrossRef]

33. Sandi, S.G.; Saco, P.M.; Rodriguez, J.F.; Saintilan, N.; Wen, L.; Kuczera, G.; Riccardi, G.; Willgoose, G. Patch organization and resilience of dryland wetlands. *Sci. Total Environ.* **2020**, *726*, 138581. [CrossRef] [PubMed]
34. Bevington, A.E.; Twilley, R.R.; Sasser, C.E. Deltaic floodplain wetland vegetation dynamics along the sediment surface elevation gradient and in response to disturbance from river flooding and hurricanes in Wax Lake Delta, Louisiana, USA. *Geomorphology* **2022**, *398*, 108011. [CrossRef]
35. Johnson, W.C.; Volke, M.A.; Scott, M.L.; Dixon, M.D. The dammed Missouri: Prospects for recovering Lewis and Clark's River. *Ecohydrology* **2015**, *8*, 765–771. [CrossRef]
36. Shi, L.; Wang, Y.; Jia, Y.; Lu, C.; Lei, G.; Wen, L. Vegetation cover dynamics and resilience to climatic and hydrological disturbances in seasonal floodplain: The effects of hydrological connectivity. *Front. Plant Sci.* **2017**, *8*, 2196. [CrossRef] [PubMed]
37. Knox, R.L.; Wohl, E.E.; Morrison, R.R. Levees don't protect, they disconnect: A critical review of how artificial levees impact floodplain functions. *Sci. Total Environ.* **2022**, *837*, 155773. [CrossRef]
38. Roni, P.; Hall, J.E.; Drenner, S.M.; Arterburn, D. Monitoring the effectiveness of floodplain habitat restoration: A review of methods and recommendations for future monitoring. *Wiley Interdiscip. Rev. Water* **2019**, *6*, e1355. [CrossRef]
39. Jorde, K.; Burke, M.; Scheidt, N.; Welcker, C.; King, S.; Borden, C. Reservoir operations, physical processes, and ecosystem losses. In *Gravel-Bed Rivers VI: From Process Understanding to River Restoration*; Habersack, H., Piégay, H., Rinaldi, M., Eds.; Elsevier B.V.: Leinz, Austria, 2007; pp. 607–636.
40. Entwistle, N.S.; Heritage, G.L.; Schofield, L.A.; Williamson, R.J. Recent changes to floodplain character and functionality in England. *Catena* **2019**, *174*, 490–498. [CrossRef]
41. Wang, J.; Sheng, Y.; Tong, T.S.D. Monitoring decadal lake dynamics across the Yangtze Basin downstream of Three Gorges Dam. *Remote Sens. Environ.* **2014**, *152*, 251–269. [CrossRef]
42. Wang, H.; Liu, X.; Wang, H. The Yangtze River floodplain: Threats and rehabilitation. In *Fishery Resources, Environment, and Conservation in the Mississippi and Yangtze (Changjiang) River Basins*; Yushun, C., Chapman, D., Jackson, J., Zhongjie, L., Kilgore, J., Phelps, O., Eggleton, M., Eds.; American Fisheries Society: Bethesda, MD, USA, 2016; Volume 84, pp. 263–291.
43. Fang, J.; Wang, Z.; Zhao, S.; Li, Y.; Tang, Z.; Yu, D.; Ni, L.; Liu, H.; Xie, P.; Da, L.; et al. Biodiversity changes in the lakes of the Central Yangtze. *Front. Ecol. Environ.* **2006**, *4*, 369–377. [CrossRef]
44. Du, Y.; Xue, H.P.; Wu, S.J.; Ling, F.; Xiao, F.; Wei, X.H. Lake area changes in the middle Yangtze region of China over the 20th century. *J. Environ. Manag.* **2011**, *92*, 1248–1255. [CrossRef] [PubMed]
45. Feng, L.; Han, X.; Hu, C.; Chen, X. Four decades of wetland changes of the largest freshwater lake in China: Possible linkage to the Three Gorges Dam? *Remote Sens. Environ.* **2016**, *176*, 43–55. [CrossRef]
46. Zhang, G.; Yao, T.; Chen, W.; Zheng, G.; Shum, C.K.; Yang, K.; Piao, S.; Sheng, Y.; Yi, S.; Li, J.; et al. Regional differences of lake evolution across China during 1960s–2015 and its natural and anthropogenic causes. *Remote Sens. Environ.* **2019**, *221*, 386–404. [CrossRef]
47. Chen, T.; Wang, Y.; Gardner, C.; Wu, F. Threats and protection policies of the aquatic biodiversity in the Yangtze River. *J. Nat. Conserv.* **2020**, *58*, 125931. [CrossRef]
48. Liu, X.; Wang, H. Effects of loss of lateral hydrological connectivity on fish functional diversity. *Conserv. Biol.* **2018**, *32*, 1336–1345. [CrossRef]
49. Dudgeon, D. Requiem for a river: Extinctions, climate change and the last of the Yangtze. *Aquat. Conserv. Mar. Freshw. Ecosyst.* **2010**, *20*, 127–131. [CrossRef]
50. Dronova, I. Object-based image analysis in wetland research: A review. *Remote Sens.* **2015**, *7*, 6380–6413. [CrossRef]
51. Han, X.; Chen, X.; Feng, L. Four decades of winter wetland changes in Poyang Lake based on Landsat observations between 1973 and 2013. *Remote Sens. Environ.* **2015**, *156*, 426–437. [CrossRef]
52. Mohammadi, A.; Costelloe, J.F.; Ryu, D. Application of time series of remotely sensed normalized difference water, vegetation and moisture indices in characterizing flood dynamics of large-scale arid zone floodplains. *Remote Sens. Environ.* **2017**, *190*, 70–82. [CrossRef]
53. Chapple, D.; Dronova, I. Vegetation development in a tidal marsh restoration project during a historic drought: A remote sensing approach. *Front. Mar. Sci.* **2017**, *4*, 243. [CrossRef]
54. Shuman, C.S.; Ambrose, R.F. A comparison of remote sensing and ground-based methods for monitoring wetland restoration success. *Restor. Ecol.* **2003**, *11*, 325–333. [CrossRef]
55. Sims, N.C.; Colloff, M.J. Remote sensing of vegetation responses to flooding of a semi-arid floodplain: Implications for monitoring ecological effects of environmental flows. *Ecol. Indic.* **2012**, *18*, 387–391. [CrossRef]
56. Shaeri Karimi, S.; Saintilan, N.; Wen, L.; Cox, J. Spatio-temporal effects of inundation and climate on vegetation greenness dynamics in dryland floodplains. *Ecohydrology* **2022**, *15*, e2378. [CrossRef]
57. Jing, L.; Lu, C.; Xia, Y.; Shi, L.; Zuo, A.; Lei, J.; Zhang, H.; Lei, G.; Wen, L. Effects of hydrological regime on development of *Carex* meadows in East Dongting Lake, a Ramsar Wetland for wintering waterbirds. *Sci. Rep.* **2017**, *7*, 41761. [CrossRef]
58. Jing, L.; Zhou, Y.; Zeng, Q.; Liu, S.; Lei, G.; Lu, C.; Wen, L. Exploring wetland dynamics in large river floodplain systems with unsupervised machine learning: A case study of the Dongting Lake, China. *Remote Sens.* **2020**, *12*, 2995. [CrossRef]
59. Long, X.; Li, X.; Lin, H.; Zhang, M. Mapping the vegetation distribution and dynamics of a wetland using adaptive-stacking and Google Earth Engine based on multi-source remote sensing data. *Int. J. Appl. Earth Obs.* **2021**, *102*, 102453. [CrossRef]

60. Yang, L.; Wang, L.; Yu, D.; Yao, R.; He, Q.; Wang, S.; Wang, L. Four decades of wetland changes in Dongting Lake using Landsat observations during 1978–2018. *J. Hydrol.* **2020**, *587*, 124954. [CrossRef]
61. Wood, S.N. *Generalized Additive Models: An Introduction with R*, 2nd ed.; Chapman and Hall/CRC Press: New York, NY, USA, 2017; pp. 1–496.
62. Braimoh, A.K. *Spatial Analysis of Residential Land Use Change in Lagos, Nigeria*; UNU-IAS Working Paper No. 144; United Nations University: Tokyo, Japan, 2006.
63. Pontius, R.G.; Shusas, E.; McEachern, M. Detecting important categorical land changes while accounting for persistence. *Agric. Ecosyst. Environ.* **2004**, *101*, 251–268. [CrossRef]
64. Okes, N.C.; Hockey, P.A.; Cumming, G.S. Habitat use and life history as predictors of bird responses to habitat change. *Conserv. biol.* **2008**, *22*, 151–162. [CrossRef]
65. Rasool, M.A.; Hassan, M.A.; Zhang, X.; Zeng, Q.; Jia, Y.; Wen, L.; Lei, G. Habitat Quality and Social Behavioral Association Network in a Wintering Waterbirds Community. *Sustainability* **2021**, *13*, 6044. [CrossRef]
66. Foga, S.; Scaramuzza, P.L.; Guo, S.; Zhu, Z.; Dilley, R.D.; Beckmann, T.; Schmidt, G.L.; Dwyer, J.L.; Joseph Hughes, M.; Laue, B. Cloud detection algorithm comparison and validation for operational Landsat data products. *Remote Sens. Environ.* **2017**, *194*, 379–390. [CrossRef]
67. Chen, B.; Chen, L.; Huang, B.; Michishita, R.; Xu, B. Dynamic monitoring of the Poyang Lake wetland by integrating Landsat and MODIS observations. *ISPRS J. Photogramm.* **2018**, *139*, 75–87. [CrossRef]
68. Bannari, A.; Morin, D.; Bonn, F.; Huete, A.R. A review of vegetation indices. *Remote Sens. Rev.* **1995**, *13*, 95–120. [CrossRef]
69. Gómez, C.; White, J.C.; Wulder, M.A.; Alejandro, P. Historical Forest biomass dynamics modelled with Landsat spectral trajectories. *ISPRS J. Photogramm.* **2014**, *93*, 14–28. [CrossRef]
70. Rouse, J.W.; Haas, R.H.; Deering, D.W.; Schell, J.A.; Harlan, J.C. *Monitoring the Vernal Advancement and Retrogradation (Green Wave Effect) of Natural Vegetation*; E73-10693; NASA: Greenbelt, MD, USA, 1973; p. 112.
71. McFeeters, S.K. The use of normalized difference water index (NDWI) in the delineation of open water features. *Int. J. Remote Sens.* **1996**, *17*, 1425–1432. [CrossRef]
72. Merzlyak, M.N.; Gitelson, A.A.; Chivkunova, O.B.; Rakitin, V.Y. Non-destructive optical detection of pigment changes during leaf senescence and fruit ripening. *Physiol. Plantar.* **1999**, *106*, 135–141. [CrossRef]
73. Huete, A.R. A Soil-adjusted vegetation index (SAVI). *Remote Sens. Environ.* **1998**, *25*, 295–309. [CrossRef]
74. Gitelson, A.A.; Merzlyak, M.N. Signature Analysis of Leaf Reflectance Spectra: Algorithm Development for Remote Sensing of Chlorophyll. *J. Plant Physiol.* **1996**, *148*, 494–500. [CrossRef]
75. Rikimaru, A.; Miyatake, S. Development of Forest Canopy Density Mapping and Monitoring Model using Indices of Vegetation, Bare soil and Shadow. In Proceedings of the 18th Asian Conference on Remote Sensing (ACRS), Kuala Lumpur, Malaysia, 20–25 October 1997.
76. Wang, C.; Chen, J.; Wu, J.; Tang, Y.; Shi, P.; Black, T.A.; Zhu, K. A snow-free vegetation index for improved monitoring of vegetation spring green-up date in deciduous ecosystems. *Remote Sens. Environ.* **2017**, *196*, 1–12. [CrossRef]
77. Fritsch, F.N.; Carlson, R.E. Monotone piecewise cubic interpolation: Algorithms and software. In Proceedings of the SIAM Fall Meeting, Houston, TX, USA, 6 November 1980.
78. Breiman, L. Statistical Modeling: The Two Cultures. *Stat. Sci.* **2001**, *16*, 199–231. [CrossRef]
79. Eisavi, V.; Homayouni, S.; Yazdi, A.M.; Alimohammadi, A. Land cover mapping based on random forest classification of multitemporal spectral and thermal images. *Environ. Monit. Assess.* **2015**, *187*, 291. [CrossRef] [PubMed]
80. Rodriguez-Galiano, V.F.; Ghimire, B.; Rogan, J.; Chica-Olmo, M.; Rigol-Sanchez, J.P. An assessment of the effectiveness of a random forest classifier for land-cover classification. *ISPRS J. Photogramm.* **2012**, *67*, 93–104. [CrossRef]
81. Mahdianpari, M.; Salehi, B.; Mohammadimanesh, F.; Brisco, B. An Assessment of Simulated Compact Polarimetric SAR Data for Wetland Classification Using Random Forest Algorithm. *Can. J. Remote Sens.* **2017**, *43*, 468–484. [CrossRef]
82. Van Beijma, S.; Comber, A.; Lamb, A. Random forest classification of salt marsh vegetation habitats using quad-polarimetric airborne SAR, elevation and optical RS data. *Remote Sens. Environ.* **2014**, *149*, 118–129. [CrossRef]
83. Wen, L.; Hughes, M. Coastal wetland mapping using ensemble learning algorithms: A comparative study of bagging, boosting and stacking techniques. *Remote Sens.* **2020**, *12*, 1683. [CrossRef]
84. Liu, M.; Shi, J.; Li, Z.; Li, C.; Zhu, J.; Liu, S. Towards Better Analysis of Deep Convolutional Neural Networks. *IEEE Trans. Vis. Comput. Graph.* **2017**, *23*, 91–100. [CrossRef]
85. Pouliot, D.; Latifovic, R.; Pasher, J.; Duffe, J. Landsat Super-Resolution Enhancement Using Convolution Neural Networks and Sentinel-2 for Training. *Remote Sens.* **2018**, *10*, 394. [CrossRef]
86. Kotsiantis, S.; Kanellopoulos, D.; Pintelas, P. Data Preprocessing for Supervised Learning. *Int. J. Comput. Sci.* **2006**, *1*, 111–117.
87. Senawi, A.; Wei, H.-L.; Billings, S.A. A new maximum relevance-minimum multicollinearity (MRmMC) method for feature selection and ranking. *Pattern Recogn.* **2017**, *67*, 47–61. [CrossRef]
88. Segura, C.; Caldwell, P.; Sun, G.; McNulty, S.; Zhang, Y. A model to predict stream water temperature across the conterminous USA. *Hydrol. Process.* **2015**, *29*, 2178–2195. [CrossRef]
89. Kuhn, M. Caret package. *J. Stat. Softw.* **2008**, *28*, 1–26.
90. Probst, P.; Wright, M.; Boulesteix, A.-L. Hyperparameters and Tuning Strategies for Random Forest. *Wiley Interdiscip. Rev. Data Min. Knowl. Discov.* **2019**, *9*, e1301. [CrossRef]

91. Poff, N.L.; Allan, J.D.; Bain, M.B.; Karr, J.R.; Prestegaard, K.L.; Richter, B.D.; Sparks, R.E.; Stromberg, J.C. The natural flow regime. *BioScience* **1997**, *47*, 769–784. [CrossRef]
92. Golyandina, N.; Korobeynikov, A.; Zhigljavsky, A. SSA Analysis of One-Dimensional Time Series. In *Singular Spectrum Analysis with R. Use R!* Springer: Berlin/Heidelberg, Germany, 2018; pp. 31–120.
93. Wood, S.N.; mgcv: Mixed GAM Computation Vehicle with Automatic Smoothness Estimation. R Package Version 1.8-23. 2018. Available online: https://cran.r-project.org/web/packages/mgcv/mgcv.pdf (accessed on 16 June 2022).
94. Cribari-Neto, F.; Zeileis, A. Beta Regression in R. *J. Stat. Softw.* **2010**, *34*, 1–24. [CrossRef]
95. Marra, G.; Wood, S.N. Practical variable selection for generalized additive models. *Comput. Stat. Data Anal.* **2011**, *55*, 2372–2387. [CrossRef]
96. Durbin, J.; Watson, G.S. Testing for serial correlation in least squares regression, 1. *Biometrika* **1950**, *37*, 409–428.
97. Landis, J.R.; Koch, G.G. The measurement of observer agreement for categorical data. *Biometrics* **1977**, *33*, 159–174. [CrossRef]
98. Huylenbroeck, L.; Laslier, M.; Dufour, S.; Georges, B.; Lejeune, P.; Michez, A. Using remote sensing to characterize riparian vegetation: A review of available tools and perspectives for managers. *J. Environ. Manag.* **2020**, *267*, 110652. [CrossRef]
99. Mu, S.; Li, B.; Yao, J.; Yang, G.; Wan, R.; Xu, X. Monitoring the spatio-temporal dynamics of the wetland vegetation in Poyang Lake by Landsat and MODIS observations. *Sci. Total Environ.* **2020**, *725*, 138096. [CrossRef]
100. Borro, M.; Morandeira, N.; Salvia, M.; Minotti, P.; Perna, P.; Kandus, P. Mapping shallow lakes in a large South American floodplain: A frequency approach on multitemporal Landsat TM/ETM data. *J. Hydrol.* **2014**, *512*, 39–52. [CrossRef]
101. Peng, H.; Xia, H.; Shi, Q.; Chen, H.; Chu, N.; Liang, J.; Gao, Z. Monitoring spatial and temporal dynamics of wetland vegetation and their response to hydrological conditions in a large seasonal lake with time series Landsat data. *Ecol. Indic.* **2022**, *142*, 109283. [CrossRef]
102. Murray, N.J.; Keith, D.A.; Simpson, D.; Wilshire, J.H.; Lucas, R.M. Remap: An online remote sensing application for land cover classification and monitoring. *Methods Ecol. Evol.* **2018**, *9*, 2019–2027. [CrossRef]
103. Hamilton, S.K.; Kellndorfer, J.; Lehner, B.; Tobler, M. Remote sensing of floodplain geomorphology as a surrogate for biodiversity in a tropical river system (Madre de Dios, Peru). *Geomorphology* **2007**, *89*, 23–38. [CrossRef]
104. Ailstock, M.S.; Norman, C.M.; Bushmann, P.J. Common reedbed *Phragmites australis*: Control and effects upon biodiversity in freshwater nontidal wetlands. *Restor. Ecol.* **2001**, *9*, 49–59. [CrossRef]
105. Clevering, O.A. Between-and within-population differences in *Phragmites australis*. *Oecologia* **1999**, *121*, 447–457. [CrossRef] [PubMed]
106. Kettenring, K.M.; Mock, K.E.; Zaman, B.; McKee, M. Life on the edge: Reproductive mode and rate of invasive *Phragmites australis* patch expansion. *Biol. Invasions* **2016**, *18*, 2475–2495. [CrossRef]
107. Saintilan, N.; Asbridge, E.; Lucas, R.; Rogers, K.; Wen, L.; Powell, M.; Colloff, M.J.; Rodriguez, J.F.; Saco, P.M.; Sandi, S.; et al. Australian forested wetlands under climate change: Collapse or proliferation? *Mar. Freshw. Res.* **2021**, *73*, 1255–1262. [CrossRef]
108. Yuan, S.; Yang, Z.; Liu, X.; Wang, H. Water level requirements of a *Carex* hygrophyte in Yangtze floodplain lakes. *Ecol. Eng.* **2019**, *129*, 29–37. [CrossRef]
109. Eller, F.; Lambertini, C.; Nguyen, L.X.; Brix, H. Increased invasive potential of non-native Phragmites australis: Elevated CO_2 and temperature alleviate salinity effects on photosynthesis and growth. *Glob. Chang. Biol.* **2014**, *20*, 531–543. [CrossRef]
110. Burger, J.; Niles, L.; Clark, K.E. Importance of beach, mudflat and marsh habitats to migrant shorebirds on Delaware Bay. *Biol. Conserv.* **1997**, *79*, 283–292. [CrossRef]
111. Jia, Y.; Jiao, S.; Zhang, Y.; Zhou, Y.; Lei, G.; Liu, G. Diet shift and its impact on foraging behavior of Siberian crane (*Grus leucogeranus*) in Poyang Lake. *PLoS ONE* **2013**, *8*, e65843. [CrossRef] [PubMed]